Sliding Wear Response of a Leaded-Tin Bronze: Influence of the Counterface Material Characteristics

J.P. Pandey and B.K. Prasad

(Submitted 7 April 1997; in revised form 9 October 1997)

Observations were made of the dry sliding wear behavior of a leaded-tin bronze against different counterface materials (stainless, EN8, and EN24 steels) over a range of applied pressures and speeds. The study showed that, in addition to sliding speed and pressure, the characteristics of the counterface materials greatly control the wear response of the bronze. The results were further substantiated by the characteristics of the wear surfaces, subsurface regions, and debris particles generated during the tests.

Keywords counterface material, leaded-tin bronze, microstructure, sliding wear response, wear mechanism

1. Introduction

Leaded-tin bronzes have been used in many tribological applications, including plain bearings (Ref 1), and remain among the most widely accepted materials for such applications. However, most studies have focused on the operational performance of the actual components (bearings) in service; little attention has been paid to the role played by the microconstituents in the bearing material on the wear characteristics of the alloy (Ref 2). In addition, an important variable governing sliding wear phenomena is the nature and microstructural characteristics of the counterface materials (Ref 3).

In view of this, the present investigation examines the response of a leaded-tin bronze under the conditions of varying applied pressures, sliding speeds, and counterface materials.

2. Experimental

2.1 *Alloy Procurement*

The bearing bronze was prepared by a liquid metallurgy route. Table 1 shows its chemical composition.

2.2 *Sliding Wear Tests*

Dry sliding wear tests were conducted on polished cylindrical test specimens (53 mm long, 8 mm in diameter) using a Cameron-Plint pin-on-disk wear test apparatus. Sliding speeds of 0.42 and 1.26 m/s were used; the counterface (disk) materials were stainless steel (type 304), EN8 steel, and EN24 steel (Table 1). Pressure on the specimens was exerted with the help of a hydraulically operated loading mechanism attached to the machine. The tests were carried out to a fixed number of disk rotations (sliding distance, 500 m). Load was increased in steps until the specimen "chipped off" or seized prior to traversing the specified sliding distance.

Wear rates were computed by the weight-loss technique using a Mettler microbalance. The temperature rise near the sliding surface of the specimens was also monitored as a function of test duration with the help of a chromel-alumel thermocouple inserted in a hole made at a distance of 1.5 mm from the sliding surface.

J.P. Pandey and **B.K. Prasad,** Regional Research Laboratory (CSIR), Bhopal 462026, India.

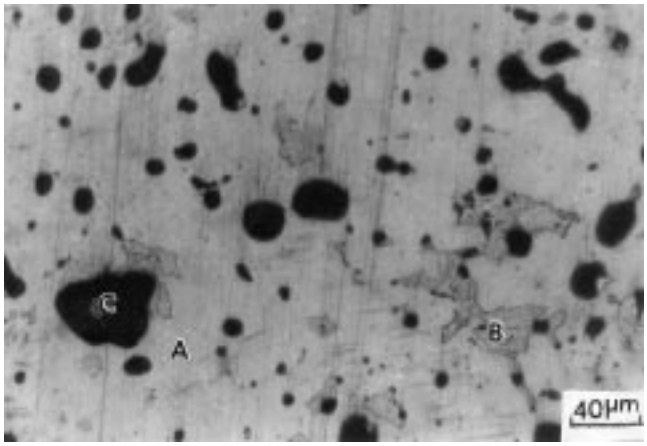

Fig. 1 Microstructural features of the bronze alloy. A, primary α; B, Cu-Sn intermetallic compound; C, lead particles

Table 1 Chemical compositions of the pin and disk materials

		Composition, wt%									
Material	**Pin/disk**	**C**	**Si**	**Mn**	**Cr**	**Mo**	**Ni**	**Fe**	**Cu**	**Pb**	**Sn**
Bronze	Pin	…	…	…	…	…	…	…	bal	15.5	7.0
EN8 steel	Disk	0.43	0.20	0.80	…	…	…	bal	…	…	…
EN24 steel	Disk	0.53	0.25	0.80	1.1	0.30	1.50	bal	…	…	…
Stainless steel (type 304)	Disk	0.14	0.85	0.82	19.50	…	9.70	bal	…	…	…

2.3 *Microscopy*

Wear surface, subsurface, and debris analyses of selected specimens were carried out using a JEOL 35CF scanning electron microscope (SEM). Bronze and steel samples were polished metallographically and etched with potassium dichromate solution and nital, respectively, for microstructural investigations conducted with a Leitz optical microscope.

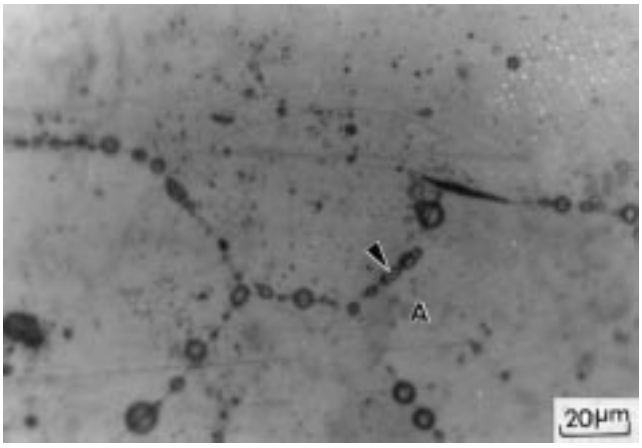

(a)

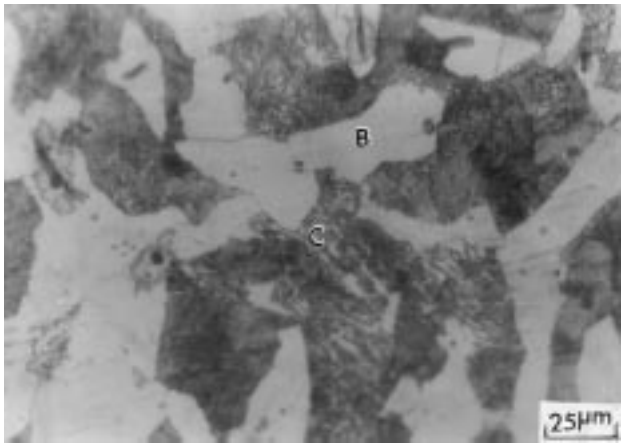

(b)

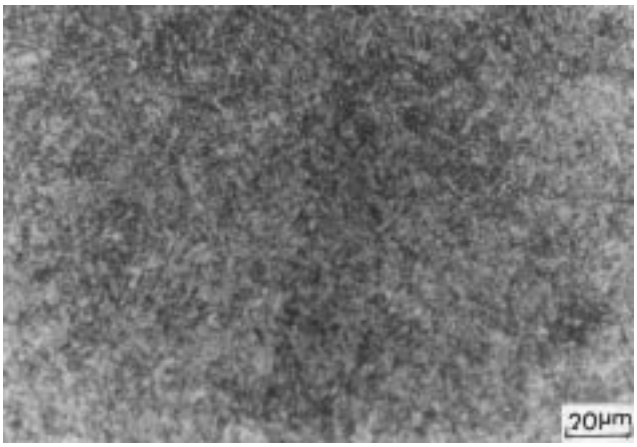

(c)

Fig. 2 Microstructural features of the disk materials. (a) Stainless steel. Arrow, carbide particles; A, austenite. (b) EN8 steel. B, ferrite; C, pearlite. (c) EN24 steel

3. Results

3.1 *Microstructure*

Figure 1 shows the microstructural features of the bronze. Areas of primary α, Cu-Sn intermetallic compound, and discrete particles of lead are indicated.

The microstructures of the counterface materials are shown in Fig. 2. The stainless steel disk contained grains of austenite and a limited quantity of carbide phases along the grain boundaries (Fig. 2a). The EN8 steel was ferrite plus pearlite (Fig. 2b). The EN24 steel disk was delineated by fine tempered martensite (Fig. 2c).

3.2 *Sliding Wear Rate*

Figure 3 shows the wear rate of the bronze as a function of applied pressure when tested at sliding speeds of 0.42 and 1.26 m/s. The influence of the disk material is also apparent. In all

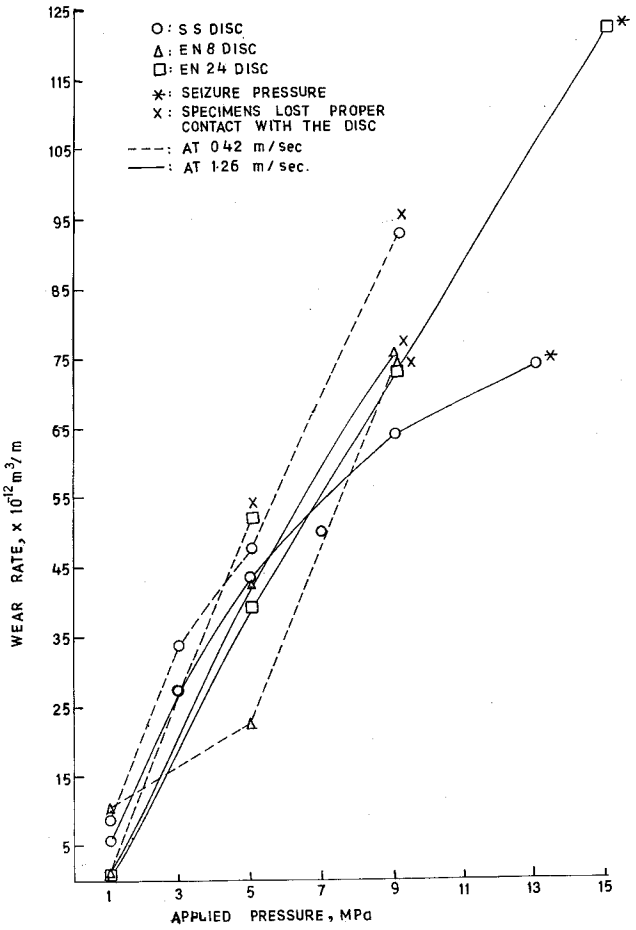

Fig. 3 Wear rate as a function of applied pressure against different disk materials

the cases, wear rate increased with speed. "Chipping off" of material was observed for the alloy regardless of the type of disk in the pressure range of 5.0 to 9.0 MPa at a sliding speed of 0.42 m/s. Furthermore, wear rate reached a maximum for the EN24 steel counterface and was lowest for the EN8 steel disk. The stainless steel counterface produced intermediate wear rates.

Chipping of the bronze also occurred when tests were conducted against the EN8 steel disk at a sliding speed of 1.26 m/s in a manner similar to that at 0.42 m/s. The wear rate of the bronze specimen reached a maximum for the stainless steel disk at lower applied pressures and was lowest for the EN24 steel disk. The EN8 steel disk produced intermediate wear rates.

3.3 *Temperature Rise*

Figure 4 shows the temperature rise near the bronze specimen surface as a function of test duration at different pressures

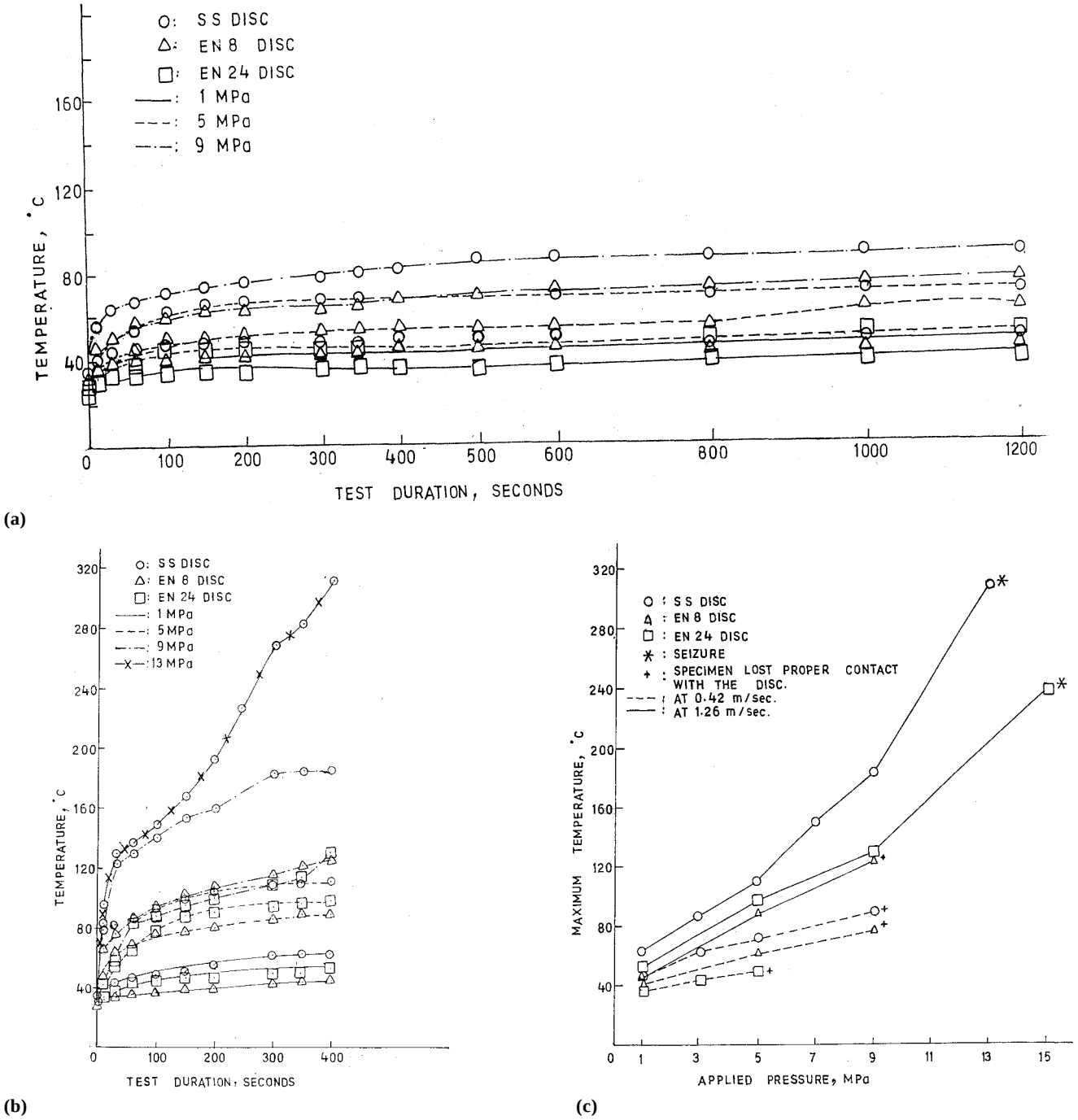

Fig. 4 Temperature rise as a function of test duration at 0.42 m/s (a) and 1.26 m/s (b) against different disk materials. (c) Maximum temperature rise as a function of applied pressure at both speeds against different disk materials

and speeds against different counterfaces. The rate of temperature increase was considerably larger at the beginning of the tests. This was followed by a lower rate of temperature rise at longer test durations.

At a sliding speed of 0.42 m/s, the degree of frictional heating reached a maximum when the stainless steel disk was used; the EN24 steel disk caused minimum heating. The EN8 steel disk produced an intermediate temperature rise (Fig. 4a).

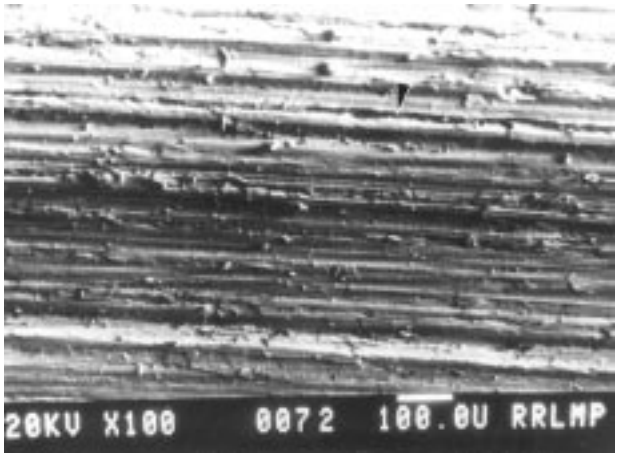

(a)

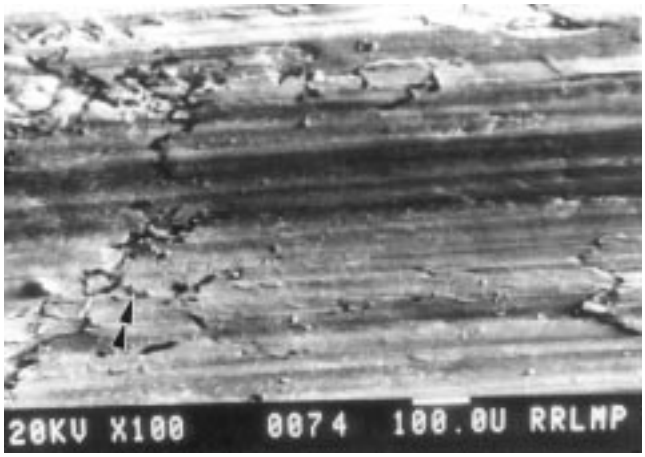

(b)

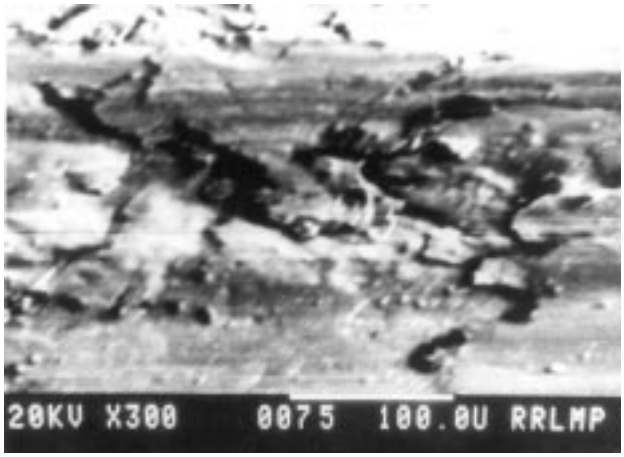

(c)

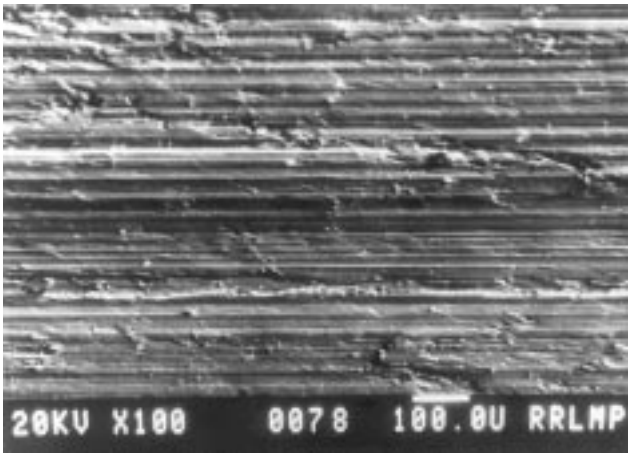

(d)

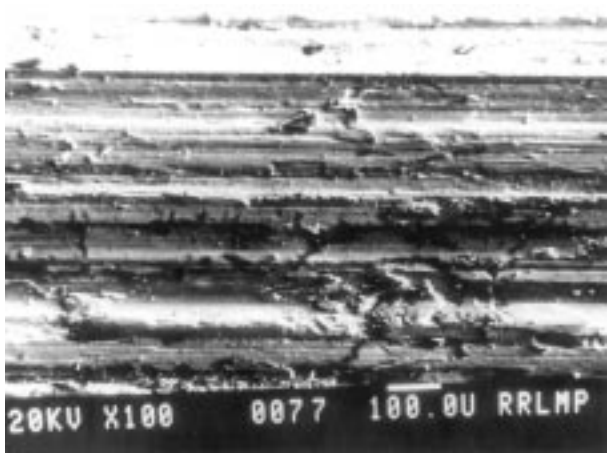

(e)

Fig. 5 SEM micrographs of the wear surfaces of the bronze alloy at different sliding speeds and pressures when tested against the EN24 steel disk. (a) 1.0 MPa at 0.42 m/s. Arrow, deeper grooves. (b and c) 5.0 MPa at 0.42 m/s. Double arrow in (b), microcracks. (d) 1.0 MPa at 1.26 m/s. (e) 15.0 MPa at 1.26 m/s

At a sliding speed of 1.26 m/s and lower pressures, the specimens experienced minimum frictional heating when the EN8 steel disk was the counterface. The stainless steel disk produced the maximum degree of heating, and the EN24 steel disk resulted in intermediate values (Fig. 4b).

Figure 4(c) compares maximum temperature rise as a function of applied pressure at both speeds for different counterface materials. At 0.42 m/s, the stainless steel disk caused the maximum degree of frictional heating, the EN24 steel disk the least, and the EN8 steel disk an intermediate extent. The EN8 steel disk produced a somewhat lower degree of heating than the EN24 steel disk at 1.26 m/s; at this speed, however, the stainless steel disk again caused the maximum degree of frictional heating.

3.4 *Wear Surfaces*

Figure 5 shows the wear surfaces of the bronze specimens tested using the EN24 steel disk as a counterface. The wear surface at a sliding speed of 0.42 m/s at low applied pressures revealed a few deeper grooves (Fig. 5a). The extent of plastic deformation in this case was marginally small. On the other hand, higher applied pressures at the same speed generated wear surfaces with increased damage (Fig. 5b and c). Microcracking on the wear surface was also observed (Fig. 5b).

The extent of plastic deformation and surface damage at 1.26 m/s at low applied pressures (Fig. 5d) was similar to that observed at 0.42 m/s. However the tendency of the bronze to crack at this speed was reduced somewhat (Fig. 5e).

3.5 *Subsurface Regions*

The subsurface regions of the bronze at different speeds and pressures are shown in Fig. 6. Note that to a considerable extent subsurface cracks were generated in the specimens tested at 0.42 m/s even at minimum applied pressures (Fig. 6a). The degree of cracking increased with pressure at this speed (Fig. 6b). The regions marked A are in the process of being detached to form wear debris. Limited flow of material in the direction of sliding was also observed near the wear surface.

Microcracking in the subsurface regions decreased to some extent at 1.26 m/s at low pressures (Fig. 6c), whereas the extent of plastic deformation was marginally greater at higher pressures (Fig. 6d and e) when compared with specimens tested at 0.42 m/s. The flow of microconstituents, including lead particles, is noticeable at the 1.26 m/s sliding speed (Fig. 6c and d).

3.6 *Wear Debris*

Debris particles from the bronze specimen when tested against the EN24 steel disk at different sliding speeds and pressures are shown in Fig. 7. At 0.42 m/s, the debris was flaky and quite large at low pressures (Fig. 7a), further increasing in size at higher pressures (Fig. 7b and c). In fact, in the latter case the debris was much coarser than shown, and also revealed the presence of microcracks. Interestingly, the debris size shrank considerably at a sliding speed of 1.26 m/s, especially at higher pressures (Fig. 7e); however, at lower pressures and the same speed (Fig. 7d), debris size was similar to that formed at 0.42 m/s.

4. Discussion

4.1 *Microstructure*

The bronze contained a considerable amount of tin and lead (Table 1). It has been observed that lead attains negligible solid solubility with copper and tin (Ref 4, 5). This leads to the formation of discrete particles of lead in the alloy (Fig. 1, region C). On the contrary, tin has considerable solid solubility with copper, as a result of which Cu-Sn complex intermetallic compounds are formed in the matrix of α (Fig. 1, region B) when the quantity of tin in the alloy exceeds its solubility limit (Ref 6). Coring tendency of the alloy also causes the same to a limited extent even if the solubility limit is not exceeded (Ref 6).

The solid solution of tin in copper solidifies first in the form of primary α-dendrites. In the process, the excess soluble tin is rejected by the α-phase to the surrounding liquid. When the temperature decreases and the situation is favorable, Cu-Sn intermetallic compounds are formed in the interdendritic regions (Ref 6). Lead, with the lowest melting point of all elements, solidifies last as discrete particles (Fig. 1, region C).

4.2 *Wear Behavior*

The wear response of the bronze specimen can be correlated with its microstructural features, as well as with those of the counterface materials. The bronze comprised lead particles along with the Cu-Sn intermetallic compound and the α-phase. Lead is expected to smear on the specimen surface during sliding and produce lubricating effects, causing lower wear rates (Ref 7-11). On the other hand, the hard intermetallic compound carries load in the process of wear.

The α-phase provides the required compatibility and support to the load-bearing intermetallic phase and the solid lubricant particles of lead (Ref 12), enabling the smearing of the lead particles. However, it requires a specific degree of frictional heating wherein the matrix becomes viscoplastic and reduces the microcracking tendency of the alloy. As a result, lead becomes able to perform the role of a solid lubricant (Ref 7, 8).

In the absence of a sufficient degree of heating, the alloy becomes susceptible to microcracking, and cracks preferably nucleate and propagate at and along the lead/matrix interfacial regions (Ref 7, 12). Under these circumstances, lead particles are engulfed by the coarser debris particles, thereby failing to smear and lubricate the surface (Ref 13, 14), and the alloy exhibits increased wear rates (Fig. 3). In such cases, lead particles behave as weak points in the matrix—similar to graphite particles in metal-matrix composites (Ref 13), wherein the presence of graphite leads to considerably higher alloy wear rates (Ref 15).

At 0.42 m/s, chipping of material led to the generation of physically visible flaky debris. As a result, the specimens lost proper contact with the disk (Ref 12) due to the microcracking tendency of the bronze alloy (Fig. 5b, 6a and b) imparted by lead.

At the higher sliding speed of 1.26 m/s, the microcracking tendency of the bronze was suppressed to a limited extent and the degree of plastic deformation increased (Fig. 5e and 6e). This caused lower wear rates at this speed (Fig. 3), also evident from the higher degree of frictional heating (Fig. 4b) and finer debris formation (Fig. 7e).

The stainless steel disk attained minimum hardness (194 HV), followed by the EN8 and EN24 steel disks (212 and 305 HV, respectively). At a sliding speed of 0.42 m/s, the stainless steel (softest) disk produced the greatest wear rates for the bronze alloy, followed by the EN8 and EN24 steel disk. The EN24 disk, having highest hardness, resulted in the best wear

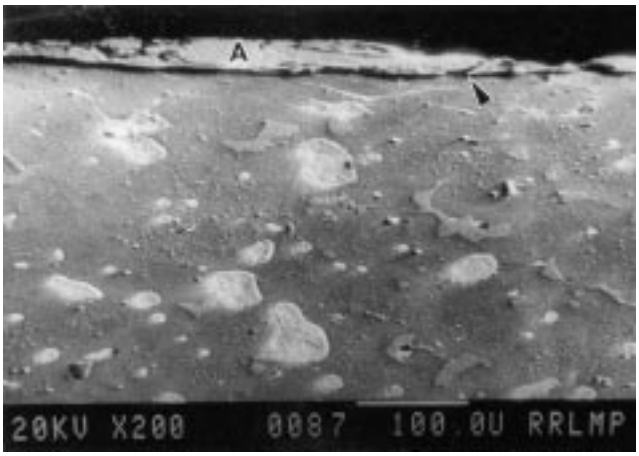

(a)

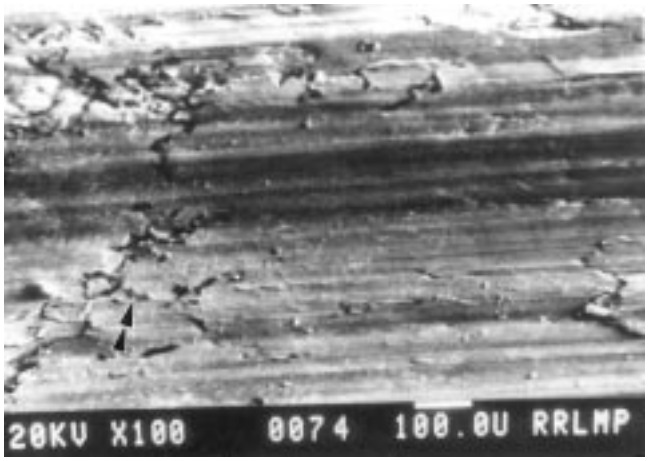

(b)

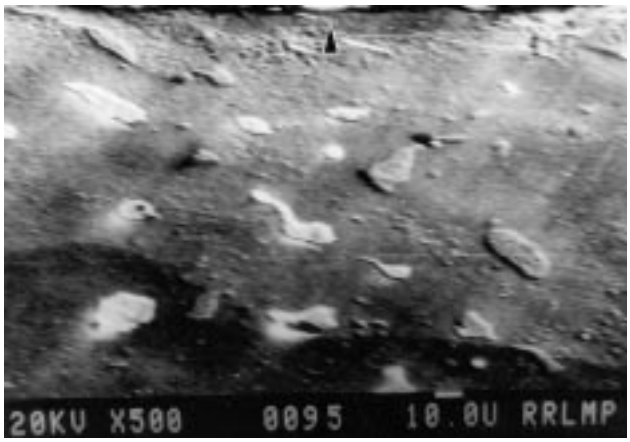

(c)

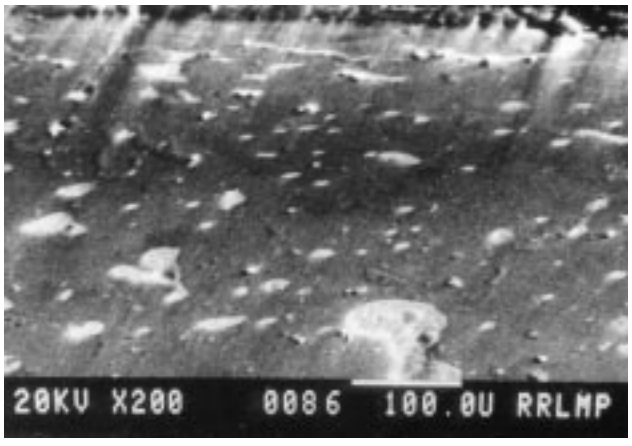

(d)

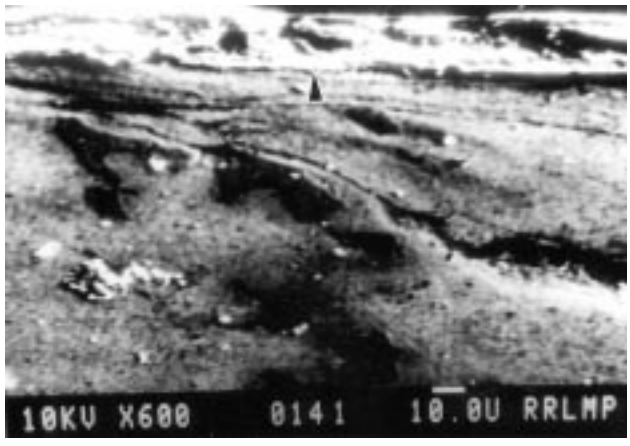

(e)

Fig. 6 SEM micrographs of the subsurface regions of the bronze alloy at different sliding speeds and pressures when tested against the EN24 steel disk. (a) 1.0 MPa at 0.42 m/s. (b) 5.0 MPa at 0.42 m/s. (c) 1.0 MPa at 1.26 m/s. (d and e) 15.0 MPa at 1.26 m/s. Regions marked A in (a) and (b) are in the process of being detached from the wear surface. Arrows in (c) and (e) indicate microcracks.

resistance at 0.42 m/s. At 1.26 m/s and higher applied pressures, however, the alloy performed best in terms of wear rates when tests were conducted using the stainless steel disk. The EN8 steel disk seemed to be the most inferior match for the bronze alloy at this speed.

The principal material-removal mechanism of the bronze was delamination of the wear surface (in view of the microcracking tendency of the alloy). This also was supported by negligible wear-induced plastic deformation observed in the subsurface region. Under the circumstances, a stable transfer

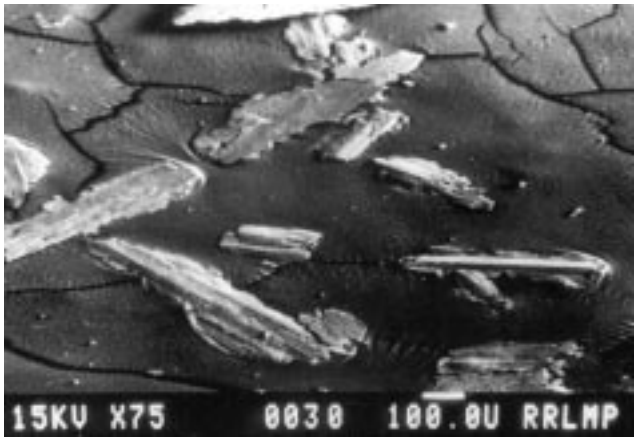

(a)

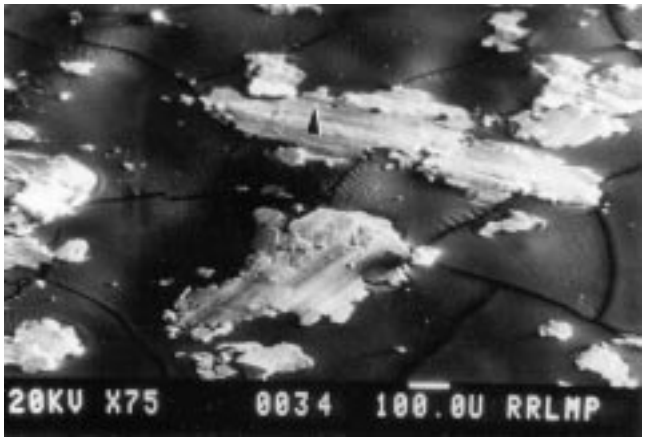

(b)

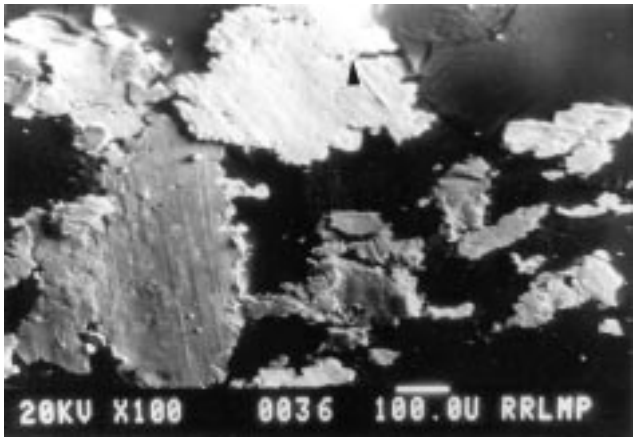

(c)

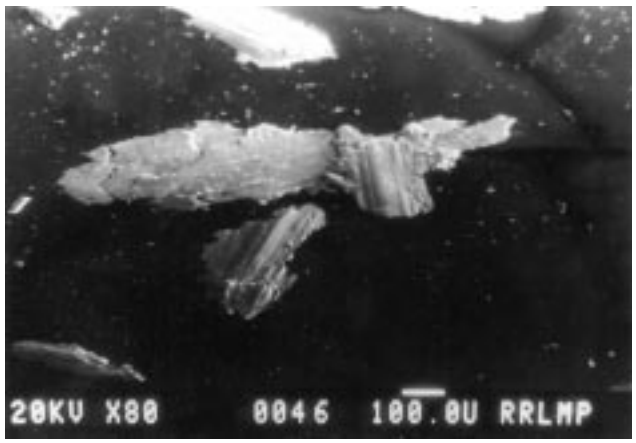

(d)

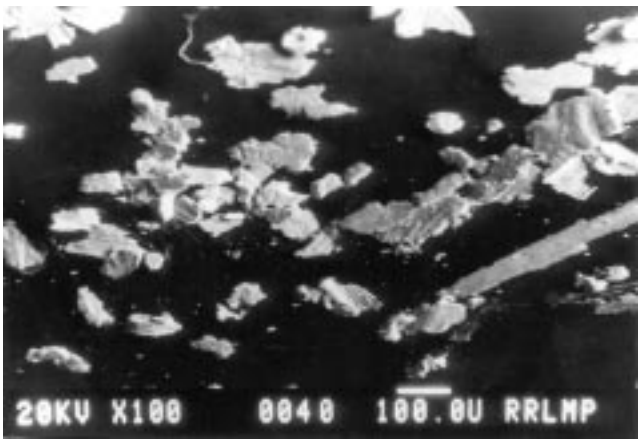

(e)

Fig. 7 SEM micrographs of the wear debris of the bronze alloy at different sliding speeds and pressures when tested against the EN24 steel disk. (a) 1.0 MPa at 0.42 m/s. (b and c) 5.0 MPa at 0.42 m/s. (d) 1.0 MPa at 1.26 m/s. (e) 15.0 MPa at 1.26 m/s. Arrows in (b) and (c) indicate microcracks.

layer does not form; thus, wear behavior deteriorates because of the premature removal of material from the surface.

5. Conclusions

Comparison of the wear performance of the bronze alloy against different disk materials shows the EN8 steel disk to be best suited at a low sliding speed. The other two disks behaved similarly to each other. The superior performance of the EN8 steel can probably be attributed to the reduced microcracking tendency of the alloy and an optimum degree of pin-disk interaction. The study indicates that when selecting a bearing material for specific applications, it is essential to consider the characteristics of the disk material(s) in addition to other working parameters in order to realize longer component life.

Acknowledgment

The authors are grateful to Prof. T.C. Rao, Director at RRL Bhopal, for his encouragement and for granting permission to publish this paper.

References

1. G.C. Pratt, *Int. Met. Rev.*, Vol 18, 1973, p 1
2. S. Das and B.K. Prasad, *Wear*, Vol 162, 1993, p 64
3. A.R. Lansdown and A.L. Price, Ed., *Materials to Resist Wear: A Guide to Their Selection and Use*, Pergamon Press, Oxford, 1986, p 23
4. E. Rabinowicz, Ed., *Friction and Wear of Materials*, John Wiley & Sons, 1965, p 114
5. W.A. Glaeser, in *Proc. Int. Conf. Wear of Materials*, Vol I, K.C. Ludema, Ed., American Society of Mechanical Engineers, 1989, p 225
6. C.R. Brooks, Ed., *Heat Treatment, Structure and Properties of Nonferrous Alloys*, American Society for Metals, 1982, p 275
7. W.A. Glaeser, in *Proc. Int. Conf. Wear of Materials*, Vol II, K.C. Ludema, Ed., American Society of Mechanical Engineers, 1989, p 225
8. J. Gerkema, *Wear*, Vol 102, 1985, p 241
9. J.P. Pathak and S.N. Tiwari, *Wear*, Vol 155, 1992, p 37
10. V.E. Buchanan, P. Molian, T. Sudarshan, and A. Akers, *Wear*, Vol 146, 1991, p 257
11. B.K. Prasad, A.K. Patwardhan, and A.H. Yegneswaran, *Mater. Sci. Technol.*, Vol 12, 1996, p 427
12. B.K. Prasad, Ph.D. thesis, University of Roorkee, Roorkee, India, 1994
13. B.S. Mazumdar, A.H. Yegneswaran, and P.K. Rohatgi, *Mater. Sci. Eng.*, Vol 68, 1984, p 85
14. S. Das, S.V. Prasad, and T.R. Ramachandran, *Mater. Sci. Eng.*, Vol 144A, 1991, p 229
15. B.K. Prasad and S. Das, *Mater. Sci. Eng.*, Vol 138A, 1991, p 123